

Electrical and Microstructural Properties of Silver Thin Films

Shiva L. U^{1*}, N. H. Ayachit¹ and Udachan L. A²

¹ Department of Physics, Rani Channamma University, Belagavi-591 156, Karnataka, India.

² Channabasaveshwar Post Graduate Studies & Research Centre, Bhalki, Dist: Bidar, Karnataka, India.

Received 13 January 2018, Revised 10 August 2018, Accepted 10 October 2018

ABSTRACT

The growth, structure and electrical properties of evaporated thin silver (Ag) films have been extensively investigated over the years because it has the highest electrical conductivity among all metals. The Ag thin films have been studied by thermal evaporation on glass, mica and Teflon. The thickness of Ag films in this investigation is in the range of 10-150 nm. The electrical properties include measurement of resistivity, the temperature coefficient of resistance (TCR), and activation energy (E_a) as a function of film thickness (t) have been studied. The experimental results are analyzed in the light of Fuchs-Sondheimer (FS) and Mayadas-Shatzkes (MS) theories. The resistivity of infinitely thick Ag film and TCR are found to be $3.53 \times 10^{-8} \Omega\text{-m}$ and $3.73 \times 10^{-3}/^\circ\text{C}$, respectively. The mean free path of conduction electron calculated from the resistivity and TCR data are 42.8 nm and 26.28 nm, respectively. A study on the initial stages of growth of Ag films and its microstructural properties has been conducted using a Scanning Electron Microscope (SEM) for films grown on different substrates and thickness.

Keywords: Thin Silver Films, Electrical Resistivity, The Electron Mean Free Path, TCR and Microstructural Properties.

1. INTRODUCTION

Ag is an extremely soft, ductile and malleable transition metal, though it is slightly less malleable than gold. Ag has a brilliant white metallic lustre that can take a high polish. Very high electrical and thermal conductivity is common to the elements in the group 11 because their single electron is free and does not interact with the filled d sub-shell, as such interactions involve lower electron mobility.

Ag is the most commonly used material in many applications because it has the highest conductivity and most reflecting. Films have to be very thin in order to preserve transparency in the visible light spectrum. New applications of transparent conductive thin films have recently been developed, leading to what now known as transparent electronics; used for flat displays, flat light sources, photovoltaic cells and smart windows. An alternative to the use of traditional Transparent Conductive Oxides (TCO) is the Indium-Tin-Oxide (ITO). The Saint-Gobain solution makes use of very thin films of Ag [1]. This is advantageous because Ag is cheaper than indium and its sourcing is more durable.

Ag is also one of the best conducting metals and widely used in the modern world for electrical conduction in multiple industries and applications, including Light-Emitting Diodes (LED), Organic Light Emitting Diodes (OLED), Flat-Panel Displays (FPD)[2], antireflection coatings [3], gas sensors [4], and as contact electrodes in solar cells [5]. Ag is used as a contact metallization

* Corresponding Author: shivaudachan8@gmail.com

in the microelectronic devices due to its low surface resistivity ($1.57 \times 10^{-8} \Omega\text{-m}$ at room temperature)[6] and its thermal stability.

Ag thin films have also been widely applied in optical applications, mainly due to high transparency and neutral colour in the visible range. Ag thin films also exhibit extremely high reflectivity in the near infrared (IR) and IR parts of the spectrum. These properties make Ag thin films an ideal candidate for low-thermal-emissivity (Low-E) coatings on glass panels, leading to energy-efficient windows for residential and commercial buildings, ultimately leading to substantial energy savings [2]. In general, the desired properties for Ag films used as metallization contacts are as follows: low specific resistivity, good thermal stability, high uniformity across the flat substrate, low particle contamination, good adherence to substrate, low manufacturing costs, and Ag has unique optical properties for topical applications such as plasmonics. The adaptive property of Ag films has been studied and employed for protein sensing with Surface-Enhanced Raman Scattering (SERS) [7].

In applications where electrical and optical properties are important; a precise measurement of thickness is required as it dictates the structure (micro/nano). The thickness of films can alter properties such as resistivity, capacitance, durability, optical wavelength, reflectivity, and opacity.

Due to the interesting properties of Ag, it is desirable to study its electrical and microstructural properties in the thin film form because the microstructure and film thickness govern the physical properties of the thin films. Thin films of Ag have been grown in a conventional vacuum coating unit with a thickness range of 50-150 nm. The electrical measurements were done in-situ by the standard four-probe technique. Microstructural analysis of Ag films also has been undertaken.

2. THEORETICAL STUDY

2.1 Electrical Conductivity and Electron Mean Free Path (l) in Bulk Ag

Theory of metallic conductivity based on average velocity was developed by Drude in 1900. Lorentz in 1905 re-investigated the problem using Boltzmann statistics. However, the use of classical statistics led to serious difficulties. Later in 1928, Sommerfeld calculated the conductivities along the line of Lorentz theory by replacing the classical statistics with Fermi-Dirac statistics. Sommerfeld did not investigate the actual mechanism of interaction between electrons and lattice any further but assumed that a relaxation time can be defined as a function of the energy of electrons only. He obtained an expression for electrical conductivity (σ) as is Equation (1) [8].

$$\sigma = \frac{ne^2\tau}{m} \quad (1)$$

where n is the concentration of electrons/ m^3 , e is the electronic charge, m is the mass of the electron, and τ is the relaxation time, which is given by $\frac{l}{V_F}$, where l is electron mean free path and V_F is velocity of electrons at the Fermi surface. It is interesting to note that although all electrons take part in the conduction mechanism however, the relaxation time of electrons only occurs at the Fermi level in conductivity.

The reason for selecting the thickness range of 50-150 nm is that the electron mean free path in bulk Ag by the electrical conductivity in Equation (1) was initially estimated as 52.5 nm.

2.2 Electrical Resistivity in Thin Films

2.2.1 Fuchs-Sondheimer (FS) Theory

The electrical response of metal thin films approaching the thickness in the range of the electron mean free path is highly affected by the electronic scattering with interfaces and defects. Fuchs worked out the detailed analysis of the size effect by solving the Boltzmann's transport equation with appropriate boundary conditions. He obtained an expression for the electrical resistivity ratio [9] as,

$$\frac{\rho_0}{\rho} = \frac{\sigma}{\sigma_0} = 1 - \frac{3}{4} \left(\lambda - \frac{\lambda^3}{12} \right) E_i(-\lambda) - \frac{3}{8\lambda} (1 - e^{-\lambda}) - \left(\frac{5}{8} + \frac{\lambda}{16} + \frac{\lambda^2}{16} \right) e^{-\lambda}$$

Where

$$-E_i(-\lambda) = \int_{\lambda}^{\infty} \left(\frac{e^{-t}}{t} \right) dt \quad (2)$$

σ_0 is conductivity of an infinitely thick film, σ is the conductivity of thin film, $\lambda = t/l$ is the ratio of film thickness, t and conduction electron mean free path, l . Equation(2) can be approximated for convenience as,

$$\rho = \rho_0 \left[1 + \frac{3}{8\lambda} \right], \quad \lambda > 0.1 \quad (3)$$

where ρ and ρ_0 are electrical resistivity of the thin and infinitely thick films respectively. There is a good agreement between Equation (3) and the exact Equation (2) [9] over a wide range of λ . However, this consideration is for total scattering. Therefore, a sophisticated theory was developed by Sondheimer [10] to measure the deviation of size effect from the bulk behavior. He introduced a specularly parameter (p), which represents the fraction of electrons, which gets specularly scattered from the film surfaces. p has the value ranging from 0 to 1. For complete specular reflection $p = 1$, the conductivity does not depend on thickness. For total diffuse scattering $p = 0$, assuming a fraction p of electrons to be specularly scattered at the surface of the film and the remaining fraction getting scattered diffusely, Equation(3) can be rewritten as,

$$\rho = \rho_0 \left[1 + \frac{3(1-p)}{8\lambda} \right], \quad \lambda > 0.1 \quad (4)$$

This expression in Equation (4) is known as Fuchs-Sondheimer equation and is extensively used to analyze experimental results. The second term on the right-hand side (RHS) of Equation (4) represents a contribution to the total resistivity (ρ) based on the size effect.

2.2.2 Mayadas-Shatzkes(MS) Theory

The Fuchs theoretical consideration did not explain the high resistivity observed in some of the thin metallic films. These thin films often have an island or grain-like structure and are discontinuous. When these grains or islands have the dimensions of the order of electron mean free path, the scattering at the grain boundaries is very high leading to high resistivity. In order to estimate the contribution of grain boundary scattering to the total film resistivity, Mayadas-Shatzkes [11] made the following assumptions:

- (i) In thin films, the individual crystal grows roughly vertically from the substrate to the upper surface of the film.

- (ii) The grain boundaries that need to be considered are those lying parallel and perpendicular to the applied field.
- (iii) The grain boundary potential could be represented by the Dirac δ - function and the dimensions of the grains are approximately equal to the electron mean free path.

In this model, the simultaneous action of these electron scattering mechanisms was considered in order to calculate the total resistivity of the metallic films. They are isotropic background scattering, surface scattering, and grain boundary scattering. Mayadas-Shatzkes solved the Boltzmann's transport equation using the above model, imposing necessary boundary conditions and finally arrived at the relation.

$$\frac{\rho_0}{\rho_g} = 3 \left[\frac{1}{3} - \frac{1}{2(\alpha')} + \alpha' \right] \text{ for small } \alpha' \quad (5)$$

Where (ρ_0/ρ_g) is the ratio of resistivity background (ρ_0) to grain boundary resistivity ρ_g , and α' is the scattering power of grain boundaries and is given by,

$$\alpha' = \frac{lR'}{d(1-R')} \quad (6)$$

Where d is the grain diameter, and R' is the grain boundary reflection coefficient. With the grain boundary scattering consideration, the total resistivity of the film becomes

$$\rho = \rho_0 \left[1 + \frac{3(1-p)}{8\lambda} + \frac{3}{2} \alpha' \right] \quad (7)$$

The third term on the right-hand side (RHS) of Equation (7) is the contribution to the total resistivity (ρ) from grain boundary scattering. Numbers of models for the electrical resistivity of thin films are given by many investigators [2,12,13].

2.3 Temperature Coefficient of Resistance-TCR (α)

Another important electrical parameter is the temperature coefficient of resistance (TCR), which is generally different in case of thin films from their bulk value. The temperature dependent part of resistivity arises from the interaction of phonons with electrons. The TCR (α_B) is defined for bulk metals as [14],

$$\alpha_B = \frac{1}{\rho_B} \frac{d\rho_B}{dT} \quad (8)$$

Similarly, for thin films, the TCR, α_t is given by

$$\alpha_t = \frac{1}{\rho_t} \frac{d\rho_t}{dT} \quad (9)$$

and we may write

$$\alpha_t \rho_t = \alpha_B \rho_B = \rho_0 \alpha_0 = \text{constant, for } \lambda \gg 1 \quad (10)$$

This equation is an alternative form of Matthiessen's rule and is independent of p . For $\lambda \ll 1$, deviation from the Matthiessen's rule is expected for all values of $p < 1$, because of the size effect. Using conductivity or resistivity expression for the thin films (F-S model), the corresponding expression for TCR from Equation (4).

$$\alpha_t = \alpha_0 \left[1 - \frac{3}{8\lambda} (1 - p) \right], \text{ for } \lambda > 0.1 \quad (11)$$

where α_t is the TCR of the thin film, α_0 is the TCR of infinitely thick film, p is the specular parameter, and λ is the ratio of film thickness (t) to the electron mean free path (l).

2.4 Activation Energy (E_a)

For metallic films, the activation energy for the thermal process, by considering the variation of resistance (R'') with temperature (T) of the film is given by [15].

$$R'' = R_0 \exp \left[\frac{E_a}{KT} \right] \quad (12)$$

Where R'' is the resistance of the film at temperature T (K), R_0 is the resistance of the film at 0 (K) and K is the Boltzmann's constant.

2.5 Thickness Dependence of Microstructure and Substrate Materials in Ag Thin Films

Nucleation and cluster formations from vapor phase will involve the condensation of vapor directly to the solid phase or via liquid phase on the surface of the substrates. The condensation of vapor atoms/molecules on an inert solid substrate takes place from a supersaturated condition of vapors. The details are discussed in the results and discussion in subsection 4.5 of section 4.

2.6 Energy Dispersive Spectroscopy, EDS Analysis

One of the most powerful attachments of SEM is Energy Dispersive X-ray Spectroscopy (EDS). Atomic qualitative and quantitative information from the specimen can be supplied by an EDS system and discussed in subsection 4.6 of section 4.

3. EXPERIMENTAL TECHNIQUE

3.1 Thermal Evaporation in a Vacuum

The vacuum coating unit used to grow thin films of Ag in this study is the Hind High Vacuum Coating Unit (Model 12A4D). The film thickness was controlled and measured by means of an in-built Quartz Crystal Digital Thickness Monitor (Model DTM-101). Ag of purity 99.99% was evaporated from amolybdenum boat at the rate of 0.5 nm/s under a vacuum of 2×10^{-6} Torr onto cleaned glass, mica and Teflon substrates at room temperature (23°C). The distance between the substrates and the evaporation source was around 0.20 m.

3.2 Substrates Cleaning Technique

Initially, the substrates were cleaned in chromic acid and then by ultrasonic. Then, the substrates were suspended in the ultrasonic wave generator tank, which contains detergent water and agitated with ultrasonic frequency. Lastly, substrates were rinsed in distilled water and dried. Substrates are then mounted on the substrate holder plate and kept in a vacuum chamber. Before deposition of the Ag films again, all the substrates were cleaned by ionic bombardment technique in the vacuum chamber. Prior to deposition of the film, the system was thoroughly degassed. The film was heated, in-situ, up to 160°C at a rate of 5°C/min.

3.3 Liquid Nitrogen Trap

The pressure inside the chamber was maintained at around 3×10^{-6} Torr during TCR measurements, using the liquid nitrogen trap. Liquid nitrogen trap provides optimum performance for the diffusion pump. Liquid nitrogen trap mounted above the diffusion pump reduces the back streaming of diffusion oil vapor and prevents oil vapors/molecules from diffusion pump from entering the system hence, provides a clean and ultimate vacuum in the chamber. Furthermore, it improves the efficiency of the system and allows it to reach low ultimate pressure.

3.4 Measurement of Resistance

The resistance measurements have been performed in-situ with the standard four-probe technique [16]. A constant current source was used to maintain a current of 0.01 mA through the film. The temperature of the film was measured by a Chromel-Alumel thermocouple held rigidly closed to the substrate. TCR measurements were taken during heating and cooling cycles.

3.5 Sample Preparation for SEM Analysis

The Ag films grown on different substrates were examined using SEM. A sample of suitable size was taken, grounded, polished and then etched using suitable etchant.

3.6 Sample Preparation for EDS Analysis

Sample preparation for EDS analysis is the same as that for SEM analysis.

4. RESULTS AND DISCUSSION

4.1 Electron Mean Free Path (l) in Bulk Ag

From the Equation (1), the electron mean free path obtained in bulk Ag is 52.5 nm. Hence, the thickness range 50-150 nm around the bulk mean free path was selected [17,18].

4.2 Electrical resistivity of thin Ag films

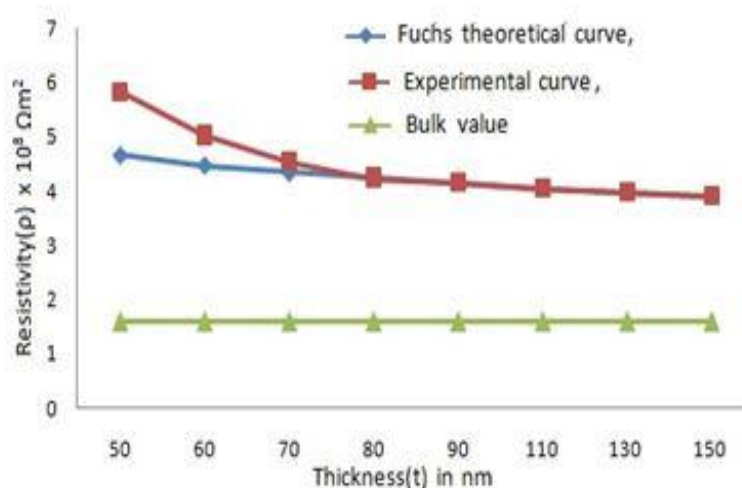


Figure 1. Variation of electrical resistivity (ρ) with thicknesses (t) for Ag films.

In Figure 1, the graph of electrical resistivity (ρ) was plotted against film thickness (t) for Ag films. The electrical resistivity is quite large for less thick films; resistivity decreases with the increasing film thickness and finally attains a constant value of about $4 \times 10^{-8} \Omega\text{-m}$ after about a thickness of 80 nm.

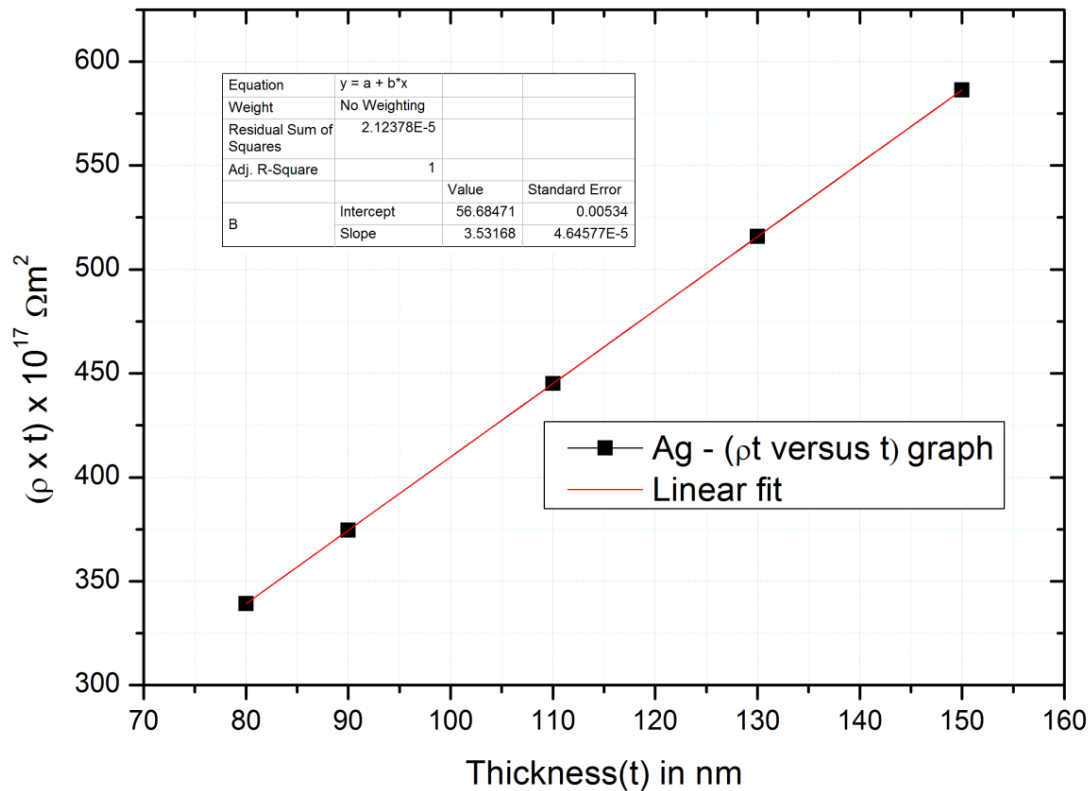


Figure 2. Plot of $(\rho \times t)$ against (t) for Ag films of thicknesses, $t > l$.

Figure 2 shows the plot of $(\rho \times t)$ versus (t) based on the Fuchs-Sondheimer in Equation (2). The graph is found to be a straight line for the thickness range from 80-150 nm. The intercept of this plot on the xis $(\rho \times t)$ yields the value of $\frac{3\rho_0 l (1-p)}{8}$ and its slope gives the value of ρ_0 , the resistivity of an infinitely thick Ag films. The values of ρ_0 and $l(1-p)$ obtained from this linear plot are $3.53 \times 10^{-8} \Omega\text{-m}$ and 42.8 nm respectively. Using these values of ρ_0 and $l(1-p)$ for total diffuse scattering (i.e. $p = 0$), we have tried to fit our experimental data, using Equation (4) by giving different values to p in the range 0 to 1. The best fit between experimental data and Fuchs - Sondheimer theoretical curve is obtained for $p = 0$. This value of p is then used to estimate the value of the electron mean free path (l), which comes out to be 42.8 nm.

The film resistivity (ρ) versus thickness (t) experimental curve does not approach the bulk value (ρ_B), $1.59 \times 10^{-8} \Omega\text{-m}$ and $1.587 \times 10^{-8} \Omega\text{-m}$ [19, 20], up to 150 nm thickness as shown in Figure 1. A saturation value of resistivity (ρ_s) about $4 \times 10^{-8} \Omega\text{-m}$ was observed after about a thickness 80 nm and found that the infinitely thick film resistivity is $3.53 \times 10^{-8} \Omega\text{-m}$. Both resistivity are comparable (i.e. ρ_s & ρ_0). Although there is a good agreement between F-S theory and our experimental points of resistivity data for higher film thicknesses, there is a wide difference between Fuchs theoretical curve and our experimental data for lower thickness films. This is because the F-S theory considers only size effects but disregards the scattering of electrons from grain boundaries. Similar type of deviation between the F-S and experimental curves for the resistivity data has been reported for other substances like palladium (Pd) [21], samarium (Sm) [22], manganese (Mn) [23], yttrium (Y) [24], ytterbium (Yb) [25], nickel (Ni) [26], tin(Sn) [27], and vanadium (V) [28].

We tried to fit our experimental data with MS theory. The theoretical curve based on MS theory is denoted by the uppermost curve in Figure 1. It is clear that there is a good agreement between the MS theory and the experimental data for thinner films where grain boundary scattering is predominant. To calculate R' , the grain diameter, d , was assumed to be equal to the thickness of the film i.e., 70 nm or below, where the experimental data deviates from the FS theoretical curve. However, for higher thicknesses (>70 nm) the grain diameter becomes very large in comparison with the mean free path of electron conduction hence, contribute to the film resistivity from the grain boundaries to become negligible. The difference between the resistivity from the F-S theoretical curve and the experimental data gives ($\frac{3\rho_0\alpha'}{2}$).

Using the values of ρ_0 and l estimated from the Fuchs theory, the value of α' and constant R' (average) were obtained as 0.155, as shown in the Table 1 below. These are used in the Equation (7) to obtain MS theoretical curve.

Table 1 Observed values of scattering power of grain boundaries (α') and grain boundary reflection coefficient (R') in silver thin films

Sl.no	Thickness (t), in nm	α'	R'	R' (average)
1	50	0.1530	0.150	0.155
2	60	0.0944	0.117	
3	70	0.1510	0.198	

α' is the scattering power of grain boundaries and is given by, Where d is the grain diameter, and R' is the grain boundary reflection coefficient.

Although there is a good agreement between Fuchs theory and our experimental points of resistivity data for higher film thicknesses, there is a wide difference between Fuchs theoretical curve and our experimental data for lower thickness films. This is because Fuchs theory only considers size effect but disregards the scattering of electrons from grain boundaries. A similar type of deviation between the Fuchs and experimental curves for the resistivity data has been reported for other substances like Sm [22], Mn [23], Yb [25], Ni [26]. Fuchs theory holds good to our experimental data for $p = 0$, indicating the total diffuse scattering of conduction electrons in Ag films. From this value of p , the electron mean free path, l was calculated as 42.8 nm which is less than l reported for bulk value, 52.5 nm. It has been reported for many metallic films such as Sm [22], Mn [23], Yb [25], and V [28], that the value of ' l ' estimated from the resistivity data is higher than that estimated from the TCR data.

4.3 Temperature Coefficient of Resistance (TCR) of Ag films:

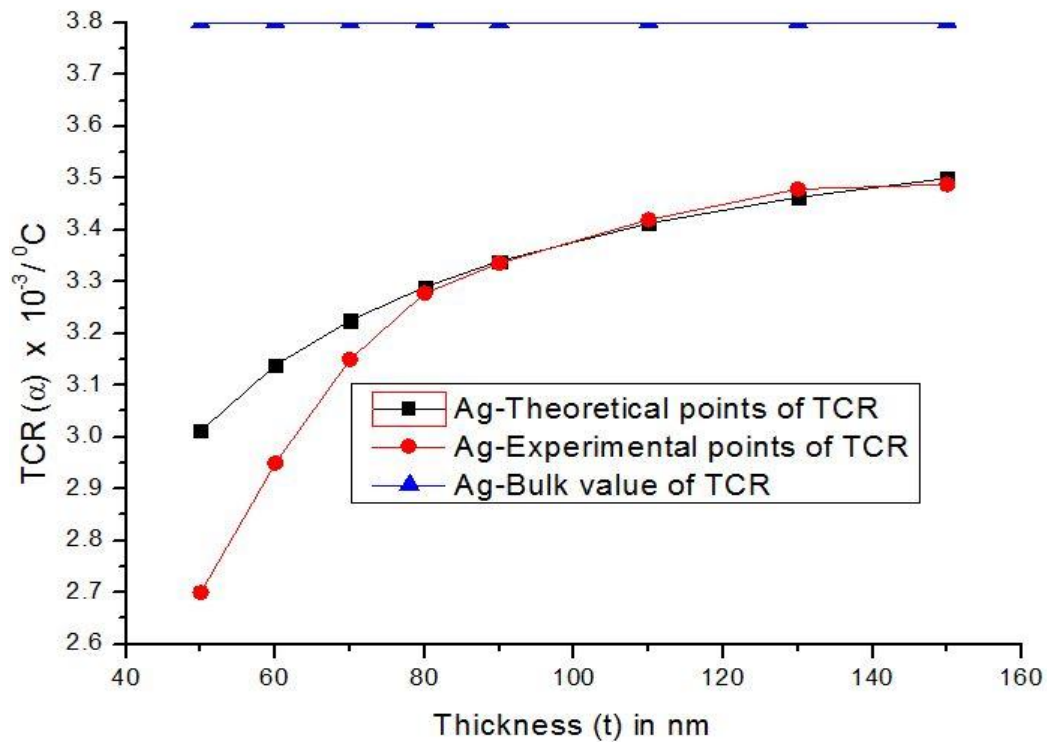


Figure 3. Variation of the temperature coefficient of resistance (α) with thickness (t) for Ag films.

The TCR (α) measurements for Ag films was conducted in the temperature range between 26-150°C. The TCR is found to be positive and thickness dependent. For lower thicknesses, the TCR has small positive value and increases as thickness increases, and finally attains a constant value of about $3.5 \times 10^{-3} / ^{\circ}\text{C}$ after a thickness of about 80 nm, as shown in Figure 3 below.

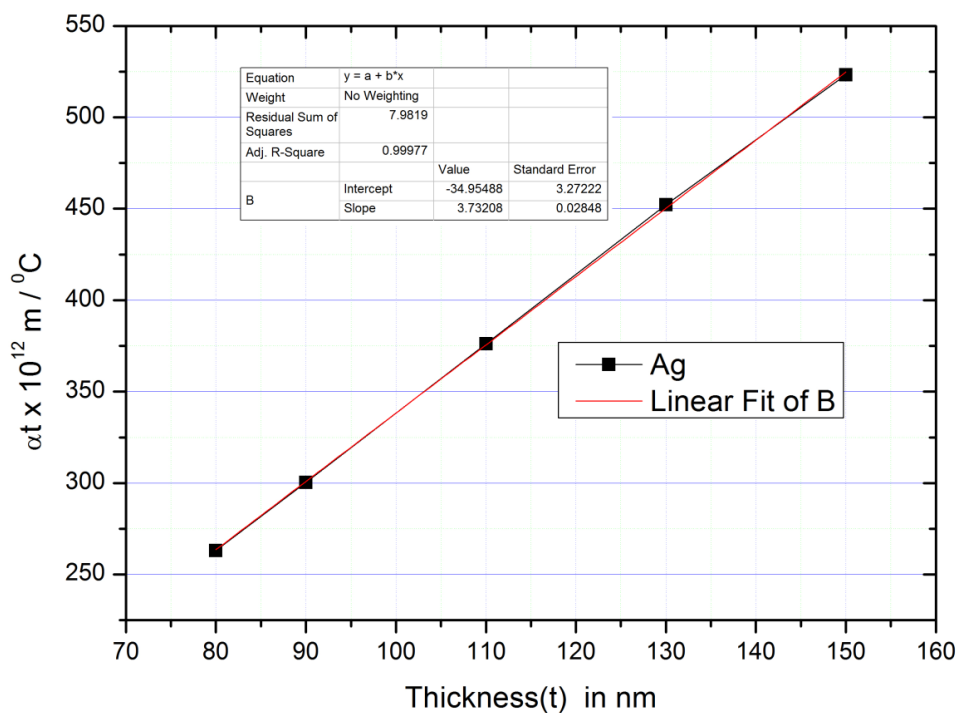


Figure 4. Plot of ($\alpha \times t$) against (t) for Ag films of thicknesses $t > l$.

Figure 4 shows the plot of $(\alpha \times t)$ against (t) based upon F-S Equation (11) for TCR. The plot is found to be a straight line with a slope (α_0) and an intercept on $(\alpha \times t)$ axis as $\frac{3\alpha_0 l (1-p)}{8}$, which have the values $3.73 \times 10^{-3}/^\circ\text{C}$ and 26.28 nm, respectively. A fairly good agreement is obtained between our experimental points and Fuchs theoretical curve for $p = 0$, for higher thicknesses. This value of p gives l as 26.28 nm. The TCR value obtained from our measurements is less than that of reported bulk value, $3.8 \times 10^{-3}/^\circ\text{C}$. The Fuchs equation for TCR curve fits our experimental data for higher thicknesses range for $p = 0$, indicating total diffuse scattering.

From our TCR and resistivity measurements on Ag films, it is found that $(\alpha \times \rho) = \text{constant}$. This indicates that the Matthiessen's rule Equation (10) is valid for Ag films. It has also been reported that Matthiessen's rule is valid for Ta [29], Ni [26], Pd [21] and Sm [22] films, since the TCR of Ag is positive and found to be a function of temperature (T).

F-S theory holds good to our experimental data for $p = 0$, indicating the total diffuse scattering of conduction electrons in Ag films. From this value of p , we have calculated the electron mean free path, $l = 26.28$ nm, which is somewhat less than that reported for bulk, where it's value is 52.5 nm.

The value of electron mean free path calculated from our resistivity data (42.8 nm) is found to be more than that of TCR data (26.28 nm). It has also been reported for many metallic films such as Yb [25], Sm [22], and Mn [23], where the value of electron mean free path (l) estimated from the resistivity data is higher than that estimated from the temperature coefficient of resistance data.

4.4 Activation Energy (E_a) of Ag

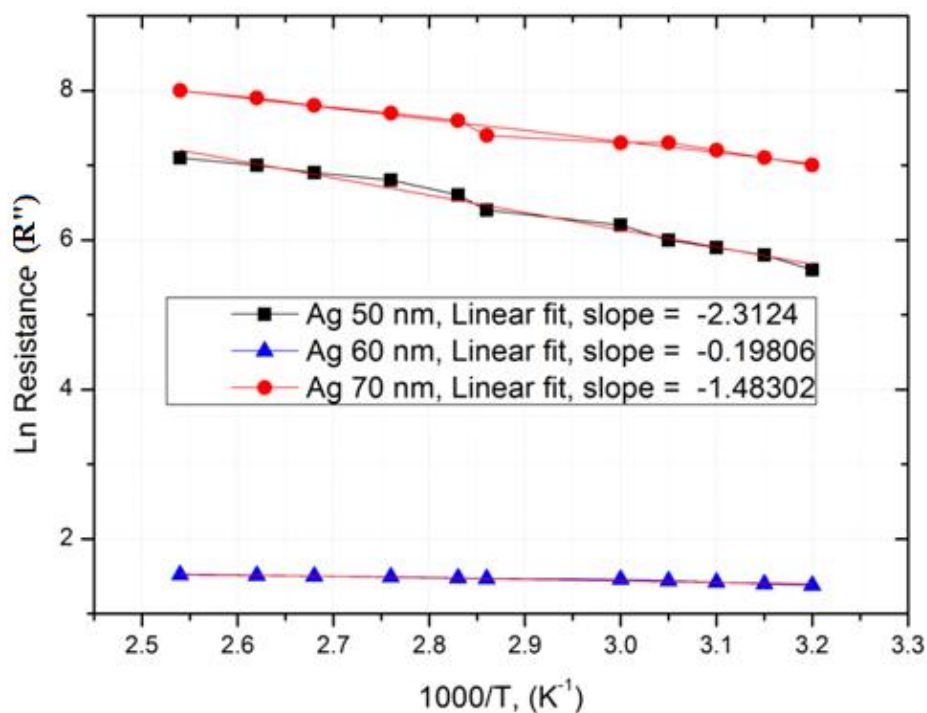


Figure 5. Plot of Ln Resistance (R'') as a function of $(1000 / T)$ for Ag films at various film thicknesses (t).

The plot of Ln R'' versus $(1000 / T)$ for various thicknesses; 50 nm, 60 nm and 70 nm are shown in Figure 5, based on Equation (12) for Ag films.

These straight lines have slope ($\frac{E_a}{K}$). The values of E_a obtained from these plots are in the range of 0.017 to 0.200 eV for Ag films, which are shown in Figure 6.

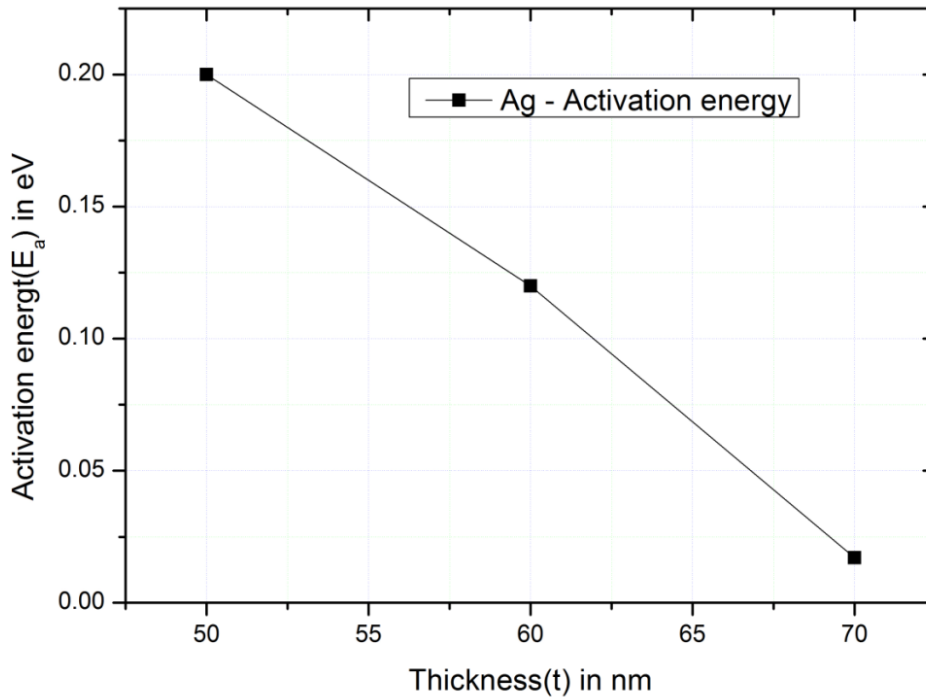


Figure 6. Plot of activation energy (E_a) against thickness (t) for Ag films.

Then we have plotted (E_a) against (t) graph (Figure 6), which shows that activation energy decreases with the increasing film thickness. During the initial stages of growth of metallic films, a particle structure has been pointed out by many researchers [30, 31]. As the deposition of the metal continues, the particle size increases by accreditation and coalescence until the particles grow together to form a continuous film. In the case of Ag films, the activation energy decreases with the film thickness increases. This is attributed by the increase of island dimensions with the increase of film thickness. The activation energies calculated for Ag films of thickness range from 50 nm to 70 nm varies from 0.017 to 0.200 eV. This type of behavior has also been observed in the case of tin [32] and in other metals.

4.5 Thickness Dependence of Microstructure and Substrate Materials in Ag Thin Films.

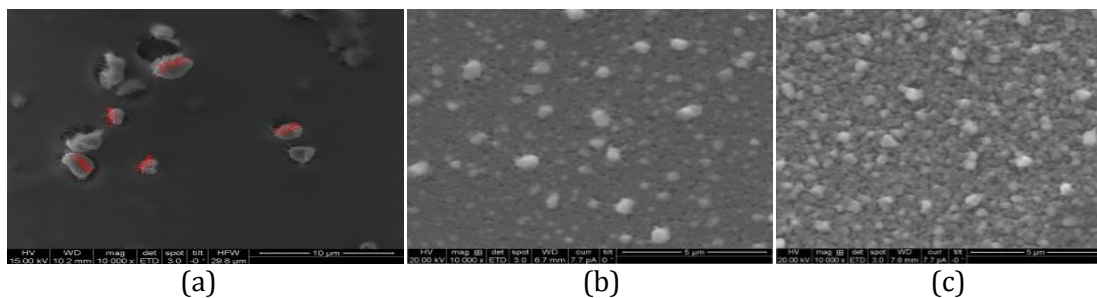


Figure 7. SEM images of Ag films with a thickness of 10 nm at 10,000x magnification for (a) Ag on the glass, (b) Ag on mica and (c) Ag on Teflon.

There are several stages in the growth process from initial nucleation to the final continuous three-dimensional formation states. The microstructure of thin films is often dictated by the environment during the film formation, the nature of the thin film deposition, substrate material

and film thickness. According to Walton [33], some critical nuclei are formed from the vapor phase on condensation at the substrate, shown in Figure 7 (a), (b) & (c) for Ag films 10 nm thickness grown on glass, mica and Teflon substrates, respectively under the same magnification.

During the growth of thin films or the formation of dispersed deposits on substrates, these films tend to adopt some atomic arrangements depending on various factors interlay crystallographic structures of the deposit and of the substrate. The morphology and microstructure of vapor deposited thin Ag films has been studied by many researchers [34,35]. The nucleation, growth and metastable-to-stable phase transformation behavior of Ag thin films were studied by means of Scanning Electron Microscopy (SEM), but most of the individual island remain as crystalline units or grains distinct separated by grain boundaries with transition regions of several thick atomic layers between different crystalline units orientation. At any constant temperature, the grain size increases with thickness. However, in the case of samples of the compound of the single Perovskite $\text{La}_{0.67}\text{Ca}_{0.33}\text{MnO}_3$, the grain size increases with temperature as stated by Mohammed *et al.* [36]. The results confirm that nucleation begins at the surface of the film and proceeds by the growth of grains as shown in Figure 7 (a), (b) and (c).

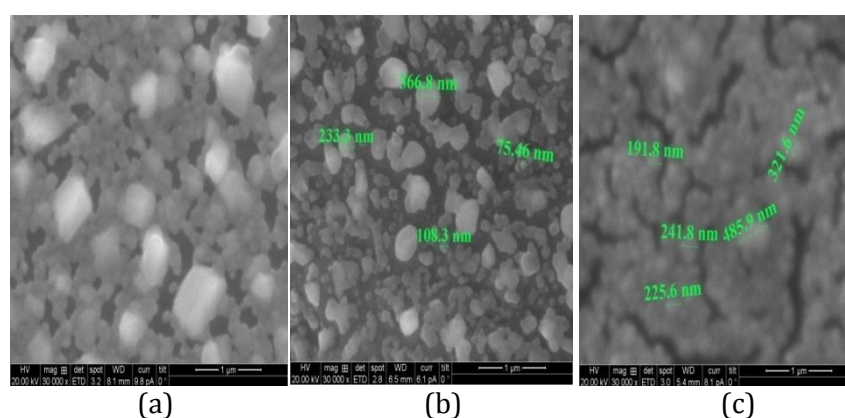


Figure 8. SEM images of Ag films of 20 nm thick at 30,000x magnification for (a) Ag on glass, (b) Ag on mica, and (c) Ag on Teflon.

As the thickness increases to 20 nm, the grain size also increases as shown in Figure 8 (a), (b) and (c). There is an interconnection of islands and hence a quasi-continuous structure was formed. The structure mainly depends on the substrate material and the binding force between substrate material and Ag deposited.

As the thickness increases, the grains grow in bigger size and elongated grain shape as shown in Figure 9 (a), (b) and (c) below due to coalescence.

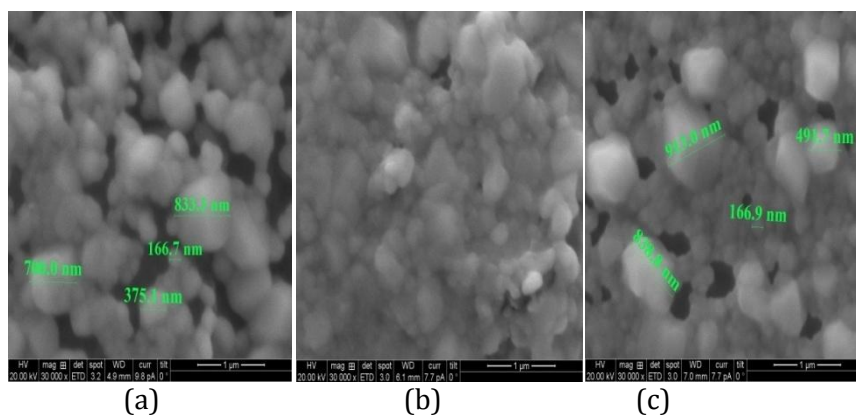


Figure 9. SEM images of Ag films of 65 nm thick at 30,000x magnification for (a) Ag on the glass, (b) Ag on mica, and (c) Ag on Teflon.

Higher island sizes are formed as the thickness of the film is increased. The islands as they grow developed some characteristic shapes and then with further growth coalescence with the neighbouring one by rounding off their edges near joining regions. The coalescence involves the considerable transfer of mass between islands by diffusion, hence, small islands disappear rapidly. During coalescence of two islands, re-crystallization takes place leading to some definite shapes of larger islands [30,35].

Figs 7, 8 and 9 show that the structure of the film depends on the substrate material, substrate roughness/smoothness, and the sticking coefficient between the substrate material and Ag films. Moreover, the substrate material happens to be one of the deposition parameters, which regulates the morphology and microstructure of Ag films. Different structures were obtained when Ag films are coated on glass, mica and Teflon substrates for the same magnification and thickness indicating the binding forces are different. It is visible that the particles are different in size when coated on different substrates for the same thickness as evidenced by Figure 9 (a), (b) and (c).

4.6 Energy Dispersive Spectroscopy, EDS Analysis

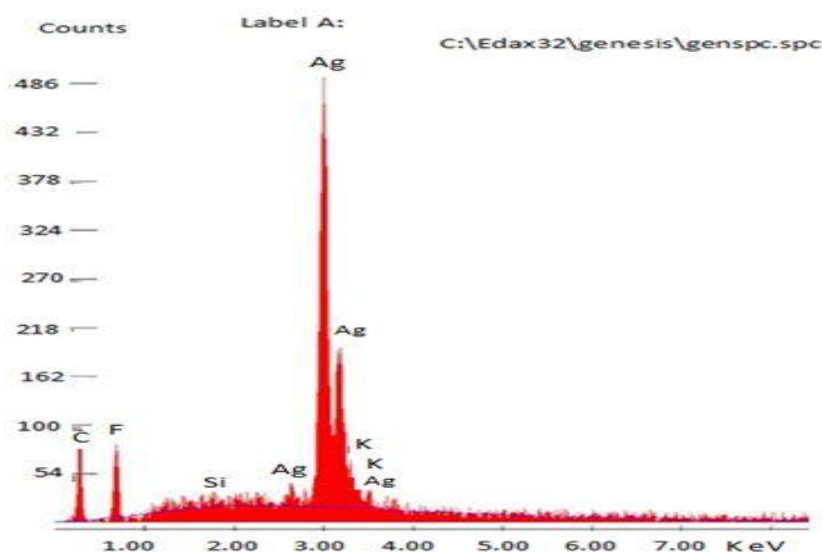


Figure 10. The EDS spectrum of a 65 nm thick of Ag with the x-axis is the energy level and y-axis is the counts (number of X-rays received and processed by the detector).

It relies on the investigation of a sample through interactions between electromagnetic radiation and matter, analyzing x-rays emitted by the matter in response to being hit with charged particles. Its characterization capabilities are due to the fundamental principle that each element has a unique atomic structure allowing a unique set of peaks on its electromagnetic emission. Figure 10 shows the EDS spectrum of Ag displays the characteristic prominent peak indicating that the material utilized in the present investigation is Ag since the Ag films are deposited on glass substrates. It is noticed in the same figure that the peaks occur at the energies of 3.2 and 3.3 eV, and the other peaks correspond to the chemical contents of the glass substrate.

In the case of nickel substituted in cadmium ferrite, prominent peaks were observed by Chavan *et al.*, 2013 [37] while checking the purity and the chemical composition of the elements using Energy Dispersive X-ray (EDX) spectrograph. The elemental composition of CdS thin films analyzed using EDS reveals peaks corresponding to cadmium and Sulphur with the appreciable intensity of cadmium peak and Sulphur peak as noticed by Pushpalata *et al.*[38].

5. CONCLUSION

The electrical and microstructural response of Ag films approaching the thickness in the range of electron mean free path and more thickness were studied theoretically as well as experimentally. The response of the thickness on the microstructure and electrical properties of Ag thin films is presented.

In very thin films, a major portion of the resistivity arises due to the scattering of the electrons at the grain boundaries, in addition to the isotropic background scattering due to the external surfaces. If the scattering mechanisms were taken into consideration, the experimental resistivity data for Ag films will closely fit the Mayadas–Shatzkes theory for the entire range of film thickness. If the scattering of grain boundaries were ignored, a wide difference in the theoretical and experimental curves is seen, particularly, in the lower thickness region for Ag films. Mathiessen's rule holds good for Ag films because of its positive TCR.

The values of electron mean free path estimated for Ag films by the measurement of resistivity and TCR are comparable with that of bulk value. Similarly, the specular parameter (p) used for fitting the experimental data with the theoretical curve is found to be the same for both resistivity and TCR data. The infinitely thick film resistivity and TCR for Ag films are of the same order of magnitude of the bulk Ag respectively. The activation energy for Ag films decreases with film thickness, as in the case of other metals.

Detailed observation has been made on the microstructure of thermally evaporated Ag films. There are several stages in the growth process from the initial nucleation of the deposits to the final continuous three-dimensional state. The stages of the film growth have been observed by SEM. From the knowledge of the initial stages of growth, one can interpret whether the film helps in the conduction of current or not and suitable for AC/DC conduction mechanism. Further, the EDS analysis study confirms that the material under investigation is Ag.

ACKNOWLEDGEMENT

The authors would like to thank DrB. G. Hegde, H.O.D. of Physics, Rani Channamma University, Belagavi, Karnataka, India for valuable discussions.

REFERENCES

- [1] Monsieur H. A., Project Cocotrans, Project ID: Anr-11-Rmnp-0010, (2011).
- [2] Guowen D., Cesar C., Daniel S., Minh L., AIP Advances **5** (2015) 117234.
- [3] Bouhafs D., Moussi A., Chikouche A., Ruiz J. M., Solar Energy Materials and Solar Cells **52** (1998) 79.
- [4] Xu J., Shun Y., Pan Q., Qin J., Sensors and Actuators, B**66** (2000) 161.
- [5] Yang L., Zhang T., Zhou H., Price S. C., Wiley B. J., You, W., American Chemistry Society Applied Material and Interfaces **3** (2011) 4075.
- [6] Zakia F., Nazir M., Ali H., American Journal of Modern Physics **3** (2014) 45.
- [7] Drachev V. P., Nashine V., Thoreson M. D., Khaliullin E. N., Ben-Amotz D., Davisson V. J., ShalaeV V. M., Lasers and Electro-Optics Society. The 17th Annual Meeting of the IEEE, (2004).
- [8] Charles K., "Introduction to Solid State Physics," Wiley India Pvt. Ltd., Seventh Edition, (2010) 158.
- [9] Larson D., "Physics of thin films," Edited by Francombe M. H., Hoffman R. W., Academic Press, New York, (1970) 84.
- [10] Sondheimer E. H., Advances in Physics **1** (1952) 1.
- [11] Mayadas A. F., Shatzkes M., Physical Review, B**1** (1970) 1382.
- [12] Horvath G., Bankuti J., Physica Status Solidi (a), **110** (1988) 549.
- [13] Gould G. N., Moraga L. A., Thin Solid Films **10** (1972) 327.
- [14] Ekertova L., "Physics of thin films," Plennm Press, New York, (1977) 168.
- [15] Goswami A., "Thin Film Fundamentals," New Age International (P) Limited Publishers, (1996) 245.
- [16] Thakur M. K., Singh O. P., Thakur K., Gaur K. S., Muhanthan N., Singh S., Singh D., Vijayan N., Singh H. K., Singh V. N., Advanced Materials Letters, **7** (2016) 525.
- [17] Shiva L. U., Ayachit N. H., Udachan L. A., Banagar A. V., Kolkundi S. S., Bhairamadagi S. S., Bulgarian Journal of Physics **45** (2018) 35.
- [18] Vyas S. M., Patel M., Thakor S., Patel V., Patel P., International Journal of Latest Technology in Engineering, Management & Applied Science **III** (2014) 166.
- [19] "Hand Book of Physics and Chemistry," Chemical Rubber Company Press, Cleveland, Ohio, 54th edition, (1974) F155.
- [20] Daniel G, Journal of Applied Sciences **119** (2016) 085101.
- [21] Shivaprasad S. M, Udachan L. A, Angadi M. A, Physics Letters **78A** (1980) 87.
- [22] Ashrit P. V, Angadi M. A, Journal of Less-Common Metals **72** (1980) 317.
- [23] Shivaprasad S. M, Ashrit P. V, Angadi M. A, Physica Status Solidi (a) **60** (1980) K159.
- [24] Ashrit P. V, Shivaprasad S. M, Angadi M. A, Thin Solid Films **72** (1980) L5.
- [25] Ashrit P. V, Angadi M. A, Physica Status Solidi (a) **63** (1981) K77.
- [26] Angadi M. A, Udachan, L. A, Thin Solid Films **79** (1981) 149.
- [27] Angadi M. A, Udachan L. A, Thin Solid Films **78** (1981) 299.
- [28] Chander R, Physica Status Solidi (a) **14** (1972) K31.
- [29] Altman C, Proceedings Nineth National Vacuum Symposium, (1962) 174.
- [30] Mohd Abdul M. K, Sushil K, Maqusood A, Salman A. A. Mohammad S. A, Nano scale research letters **6** (2011) 434.
- [31] Andressa C. S, Marcelo B. P, Flavio H, Raquel S. M, Carla R. M, Manuela P. K, Flinho F. H, Tania M. H. C, Eliana W. D. M, Edilson V. B, Journal of Brazilian Chemical Society **26** (2015) 1004.
- [32] Udachan L. A, Jogad M. S, Rama Rao S, Asian Journal of Physics **8** (1999) 207.
- [33] Walton D, Journal of Chemical. Physics. **3** (1962) 2182.
- [34] Muhammad M, Tahirzeb K, Surface Review and Letters. **12** (2005) 759.
- [35] Dimitrijević R, Cvetković O, Miodragović Z, Simić M, Manojlović D, Jovic V, Journal of Mineral Metallurgy Section B-Metal **49** (2013) B91.
- [36] Mohammed I. M, Elbadawi A. A, Abuellhassan H. H, Journal of Applied and Industrial Science **1** (2013) 12.

- [37] Chavan G. N, Papanna B, Naik L. R, Sunil Kumar, International Journal of Science and Technology Research **2** (2013) 82.
- [38] Pushpalatha H. L, Bellappa S, Narayanaswamy T. N, Ganesha R, Indian. Journal of Pure and Applied Physics. **52** (2014) 545.